ResearchGate

See discussions, stats, and author profiles for this publication at: https://www.researchgate.net/publication/45797028

Breakdown of Cell Wall Nanostructure in Dilute Acid Pretreated Biomass

ARTICLE *in* BIOMACROMOLECULES · SEPTEMBER 2010

Impact Factor: 5.75 · DOI: 10.1021/bm100455h · Source: PubMed

CITATIONS
69

READS
42

9 AUTHORS, INCLUDING:

Volker Urban
Oak Ridge National Laboratory
138 PUBLICATIONS **2,087** CITATIONS
SEE PROFILE

Arthur Ragauskas
University of Tennessee
377 PUBLICATIONS **9,660** CITATIONS
SEE PROFILE

Barbara R Evans
Oak Ridge National Laboratory
81 PUBLICATIONS **1,365** CITATIONS
SEE PROFILE

Available from: Arthur Ragauskas
Retrieved on: 24 January 2016

Breakdown of Cell Wall Nanostructure in Dilute Acid Pretreated Biomass

Sai Venkatesh Pingali,*,† Volker S. Urban,*,† William T. Heller,† Joseph McGaughey,‡ Hugh O'Neill,† Marcus Foston,§ Dean A. Myles,† Arthur Ragauskas,§ and Barbara R. Evans*,‡

Center for Structural Molecular Biology and Molecular Bioscience and Biotechnology Group, Chemical Sciences Division, Oak Ridge National Laboratory, Oak Ridge, Tennessee 37831, and Institute of Paper Science and Technology, School of Chemistry and Biochemistry, Georgia Institute of Technology, Atlanta, Georgia 30332

Received April 26, 2010; Revised Manuscript Received July 8, 2010

The generation of bioethanol from lignocellulosic biomass holds great promise for renewable and clean energy production. A better understanding of the complex mechanisms of lignocellulose breakdown during various pretreatment methods is needed to realize this potential in a cost and energy efficient way. Here we use small-angle neutron scattering (SANS) to characterize morphological changes in switchgrass lignocellulose across molecular to submicrometer length scales resulting from the industrially relevant dilute acid pretreatment method. Our results demonstrate that dilute acid pretreatment increases the cross-sectional radius of the crystalline cellulose fibril. This change is accompanied by removal of hemicellulose and the formation of $R_g \sim 135$ Å lignin aggregates. The structural signature of smooth cell wall surfaces is observed at length scales larger than 1000 Å, and it remains remarkably invariable during pretreatment. This study elucidates the interplay of the different biomolecular components in the breakdown process of switchgrass by dilute acid pretreatment. The results are important for the development of efficient strategies of biomass to biofuel conversion.

Introduction

Lignocellulosic biomass produced by terrestrial plants has the potential to be an abundant, renewable feedstock for the production of ethanol and other transportation fuels.[1,2] Of the many types of plants that have been examined as potential feedstocks for production of ethanol and other fuels, herbaceous crops, particularly grasses, offer a number of advantages. These include fast growth, established agricultural cultivation, and potential for dual-purpose production, providing both grain for food and straw (stalks) for biofuel conversion. Switchgrass (*Panicum virgatum*), a native North American prairie grass, is being developed as the main herbaceous crop for biofuel production. Switchgrass offers several advantages, including high yields, perennial growth, production of seeds, and adaptability to poor soils.[3,4]

All lignocellulosic biomass is largely composed of three component biopolymers: cellulose, a linear polymer of β-1,4-linked glucose chains assembled into partially crystalline fibers; hemicellulose, a heterogeneous branched polymer of pentose and hexose sugars; and lignin, which is composed of extensively cross-linked methoxy-substituted phenyl propane units. Cellulose, which forms the main structural component of the plant cell walls, is an attractive source of glucose for fermentative ethanol production, but must be first depolymerized by enzymatic or chemical hydrolysis. In lignocellulosic biomass, enzymatic access to the cellulose fibers is impeded by hemicellulose and lignin layers. Hydrolysis is further impeded by the crystalline, fibrous structure of cellulose.[5] As a result, efficient production of fermentable sugars from lignocellulosic biomass requires deconstruction of the plant cell walls by mechanical and chemical pretreatment.

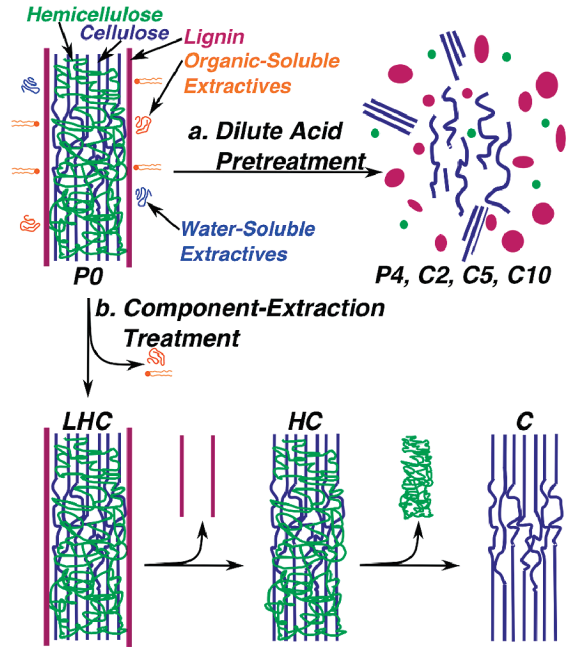

Figure 1. Schematic of (a) dilute acid pretreatment and (b) component-extraction processes.

Typically, biomass pretreatment includes size reduction by chipping and grinding, followed by chemical swelling with alkali or acid,[1,5] schematically illustrated as pathway *a* of Figure 1.[6,7] The most effective pretreatments increase the gross material

* To whom correspondence should be addressed. E-mail: pingalis@ornl.gov; urbanvs@ornl.gov; evansb@ornl.gov.
† Center for Structural Molecular Biology, Oak Ridge National Laboratory.
‡ Molecular Bioscience and Biotechnology Group, Oak Ridge National Laboratory.
§ Georgia Institute of Technology.

10.1021/bm100455h © XXXX American Chemical Society

porosity, decrease the crystallinity of the cellulose fibrils, remove hemicellulose, and reduce the lignin present.[5] Pretreatment, in addition to being a rate-limiting step, increases the cost of bioethanol production due to the high energy requirements of mechanical size reduction and heating, and incurs additional costs for responsible handling of caustic chemicals.[8−10] Soaking in dilute sulfuric acid at high temperature is a widely used biomass pretreatment method.[1] Although the efficiency of subsequent cellulose conversion to sugars by enzymatic hydrolysis is greatly increased by dilute acid pretreatment, it does not fully remove lignin, which is thought to precipitate on the cellulose surface and inhibit the hydrolysis process through a combination of binding with the cellulase enzymes and blocking the progress of the enzymes along the glucose chains.[10,11]

Although no small-angle neutron scattering work has been reported on acid pretreatment of lignocellulosic biomass, individual components of lignocellulosic biomass like native cellulose[12−21] and kraft pulp lignin[22−24] have been extensively studied. Self-assembled, synthetic cellulose fibrils produced by enzymatic polymerization were characterized at length scales ranging from nanometers to micrometers using ultra-small-angle, small-angle, and wide-angle scattering techniques.[15,19] Three observations were reported: (a) the fibrils possess a surface fractal dimension $D_s = 2.3$, indicating a slightly rough surface; (b) the material displays a mass fractal dimension $D_m = 2.1$, reflecting the internal arrangement of the self-assembled structure, and (c) the characteristic diffraction peaks of microcrystalline cellulose were observed at 2θ angles 14.9° ($1\bar{1}0$), 16.7° (110), and 22.5° (200). X-ray and neutron fiber diffraction determined the structure of the two distinct crystal phases I_α[18] and I_β[17] of naturally occurring cellulose and found remarkable differences in the crystal packing. The results show more intersheet C−H···O hydrogen bonds in the I_β form,[17] which suggests that I_β is more stable than I_α and explains the solid-state conversion $I_\alpha \rightarrow I_\beta$ by hydrothermal processes.[18,25−27]

In this paper, we report the results of studies of the structural consequences of dilute acid pretreatment of switchgrass across a wide range of length scales using small-angle neutron scattering (SANS). SANS is a powerful tool for studying bulk materials that probes length scales ranging from 10 to 10000 Å, making it ideally suited to understanding the gross morphological changes in switchgrass resulting from pretreatment. Furthermore, measurements were performed on material treated solely by a component-extraction process to better understand the impact of lignin and hemicellulose on the microstructure of switchgrass biomass. The results demonstrate that dilute acid pretreatment causes clear morphological changes in lignocellulose. The observed redistribution of lignin and removal of hemicelluloses are likely to promote penetration of enzymes into biomass.

Materials and Methods

Sample Preparation. Samples of the lowland cultivar Alamo switchgrass (*Panicum virgatum*) were harvested at Oak Ridge National Laboratory, TN. The samples were then shipped to the National Renewable Energy Laboratory (NREL) in Golden, CO, for room temperature air-drying and size-reduction. These samples were stored in a freezer to maintain the moisture content and shipped to Georgia Tech upon request. The monosaccharide and lignin content of the untreated and dilute acid pretreated samples listed in Table 1 was determined by standard procedures, as described previously.[28,29]

Switchgrass was subjected to either (i) dilute acid pretreatment (pathway *a* of Figure 1) or (ii) component-extraction treatment (pathway *b* of Figure 1).

(i) Dilute Acid Pretreated Samples. Dilute acid pretreatment of switchgrass was carried out by a modification of reported methods.[30,31]

Table 1. Compositions of the Dilute Acid Pretreated and Component-Extracted Switchgrass Samples Obtained Using Carbohydrate and Klason Lignin Analysis Approach[a]

samples	arabinose	galactose	glucose	xylose	mannose	lignin
P0	2.93	1.66	43.06	20.84	0.34	31.18
P4	3.14	1.59	42.42	22.84	0.32	29.69
C2	0.93	0.12	44.35	5.95	0.15	48.50
C5	0.32	0.12	36.08	2.54	0.11	60.83
C10	0.34	0.18	53.05	1.98	0.11	44.33
holocellulose	4.75	1.62	57.01	30.23	0.00	6.40

[a] In mass percent units.

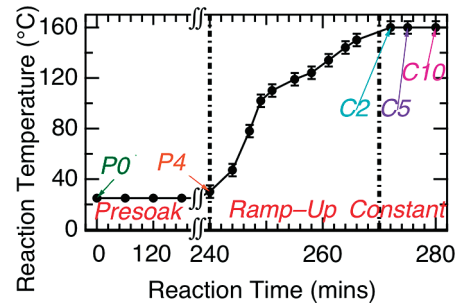

Figure 2. Reaction temperature versus reaction time of the dilute acid pretreatment of switchgrass has three phases: (i) presoak; (ii) ramp-up, and (iii) constant. Samples marked, namely, *P0* and *P4* of the presoaked phase and *C2*, *C5*, and *C10* of the constant phase, were studied using SANS.

Figure 2 illustrates the dilute acid pretreatment protocol. Untreated (*P0*): The switchgrass sample was Wiley milled to pass through 0.05 mm pore size or 20-mesh screen. Presoak (*P4*): Wiley milled switchgrass sample was presoaked at room temperature (25 °C) while continuously stirring in an ~1% dilute sulfuric acid solution at 5% dry solids (w/w) for 4 h. The presoaked slurry was filtered and the solid material was washed with an excess of deionized water to prepare sample *P4* or further treated as follows. Ramp-up: The presoaked material was transferred to a 4560 mini-Parr 300 mL pressure reactor of Parr Instrument Company in an ~1% (or 0.1−0.2 M) dilute sulfuric acid solution at 5% solids (w/w) and sealed. The impeller speed was set to ~100 rpm and the vessel was heated to 160 °C over ~30 min (at ~6 °C/min). Constant (*C2*, *C5*, *C10*): The reactor was held at 160 ± 2 °C (6.4−6.8 atm) for the specified residence time: 2, 5, and 10 min (±0.5 min). To halt the pretreatment process, the reactor was quenched in an ice bath (~5 min to cool to 70 °C). Then, the pretreated slurry was filtered to remove the solid residue and washed with an excess of deionized water and dried overnight at room temperature. All yields for biomass recovered after pretreatment ranged between 75−85% by mass of the initial material.

(ii) Component-Extracted Samples. Component-extraction of switchgrass was performed by methods previously used for preparation of poplar samples for NMR analysis.[32] Extractive-free (*LHC*): Switchgrass sample was Wiley milled to pass through 0.05 mm pore-size screen prior to extraction with benzene/ethanol (2:1, v/v) for 24 h in a Soxhlet apparatus to remove extractives. The extraction flask was refluxed at a boiling point rate, which cycled the biomass for at least 24 extractions over a 4 h period. The solvent was removed and extractive-free switchgrass was dried in air. Holocellulose isolation (*HC*): Extractive-free switchgrass samples (1.5 g) were dispersed in 125 mL of deionized water in a Kapak sealing pouch. The resulting mixture was heated in a water bath for 1 h at 75 °C prior to adding 1 mL of glacial acetic acid and 1 g of sodium chlorite ($NaClO_2$) and continuing the reaction for an additional 1 h. This procedure was repeated three times to give a total treatment time of 3 h. The treated sample was then quenched in ice-water, filtered, and washed thoroughly using deionized water and acetone before finally being air-dried overnight. This procedure was repeated to ensure complete removal of the lignin component. Chlorine dioxide is generated from $NaClO_2$ under the proper pH conditions and

lead to changes in lignin, such as degradation of the side chains, demethylation, oxidation, and depolymerization, facilitating solubilization in aqueous solution. Cellulose isolation (*C*): Holocellulose isolated switchgrass samples (1 g) were treated with 2.5 M hydrochloric acid at 100 °C for 4 h. The treated sample was washed with deionized water and acetone and air-dried to remove the hemicelluloses and obtain cellulose. Though acid-catalyzed hemicellulose removal may cause hydrolyzation of cellulose, the more facile alkaline-based procedure could cause conversion of cellulose I to cellulose II.

Small-Angle Neutron Scattering (SANS). SANS measurements were performed with the CG-3 Bio-SANS instrument[33] at the High Flux Isotope Reactor (HFIR) facility of Oak Ridge National Laboratory. All samples were soaked in 100% D_2O solvent, 2−3 times the volume of the solid sample, for over 24 h to maximize D/H exchange and solvent penetration. Soaked samples were placed in 0.5 mm thick quartz cells with detachable cell walls (Hellma Model #106-QS 0.5MM) for SANS studies. Three different instrument configurations were employed to collect data over the range of scattering vectors, 0.001 Å^{-1} < Q < 0.3 Å^{-1}, employing sample-to-detector distances of 1174 and 6874 mm, both with a neutron wavelength (λ) of 6 Å, and 15374 mm with a neutron wavelength of 18 Å. $Q = (4\pi/\lambda) \sin\theta$ and 2θ is the scattering angle. In each case the center of the area detector (Ordela 2410N) was offset by 150 mm from the beam. The instrument resolution was defined using circular aperture diameters of 40 mm for source and 8 mm for sample separated by distances: 3256 mm for 0.03 Å^{-1} < Q < 0.3 Å^{-1}, 9326 mm for 0.0065 Å^{-1} < Q < 0.06 Å^{-1}, and 17424 mm 0.001 Å^{-1} < Q < 0.009 Å^{-1}. The relative wavelength spread $\Delta\lambda/\lambda$ was set to 0.15. The scattering intensity profiles $I(Q)$ versus Q were obtained by azimuthally averaging the processed 2D images, which were normalized to incident beam monitor counts and corrected for detector dark current, pixel sensitivity, and solvent scattering backgrounds from D_2O and quartz cell.

SANS data was analyzed using the multilevel unified equation implemented in Irena Package[34] to elucidate the multiple levels of structural organization. Irena is an Igor Pro software package consisting of various structural models to analyze small-angle scattering data. For each individual level, i, the scattering signal is the sum of Guinier's exponential form and the structurally limited power-law as[35−37]

$$I(Q) = \sum_{i=1}^{n} [G_i \exp(-Q^2 R_{g_i}^2/3) + B_i \exp(-Q^2 R_{g_{(i+1)}}^2/3)\{[\mathrm{erf}(QR_{g_i}/\sqrt{6})]^3/Q\}^{P_i}] + I_{\mathrm{bkg}} \quad (1)$$

where $i = 1,.. ., n$. To model the lignocellulose SANS data, we used a total of three levels with $i = 1$ and $i = 3$ referring to the smallest and largest size structural levels, respectively. $G_i = c_i V_i \Delta\rho_i^2$ is the exponential prefactor; R_{g_i} is the radius of gyration describing the average size of the i^{th} level structural unit; B_i is a Q-independent prefactor specific to the type of power-law scattering with power-law exponent P_i and I_{bkg} is the flat background intensity due to incoherent scattering. c_i is the concentration of the i^{th} kind of particle; V_i is the volume of the particle and $\Delta\rho_i$ is the contrast of the i^{th} kind of particle with respect to the solvent. The expression of the constant prefactor is $B_i = (G_i P_i/R_g^{P_i})\Gamma(P_i/2)$ when the i^{th} level is a mass fractal composed of elementary units of the next lower, $(i-1)^{\mathrm{th}}$, level.[36]

Scanning Electron Microscopy (SEM). Switchgrass was carefully attached to adhesive carbon tape. A 3 nm thick conductive coating, applied to the surface, was found sufficient for successfully imaging the samples. Each micrograph was recorded on a Phillips XL-30 scanning electron microscope instrument with a field emission gun at an accelerating voltage of 10 kV and imaged using secondary electrons.

Results

Dilute acid pretreatment of switchgrass was carried out by a modification of previously reported methods.[30,31] The switchgrass samples were presoaked in H_2SO_4 before heating to 160 °C in a Parr Bomb reactor for different time periods to investigate structural changes that occur in the material during pretreatment (Figure 2). The chemical composition of each sample from the dilute acid pretreatment was analyzed to identify the component biopolymers remaining following treatment (see Table 1).[38] In brief, the hemicellulose content decreased from ~21 to 2%, the cellulose content increased from 43 to 53%, and the lignin content increased from 31 to 44% after a 10 min pretreatment process. It is of interest to note that the majority of the hemicellulose was solubilized after a 2 min pretreatment process (~6% remaining).

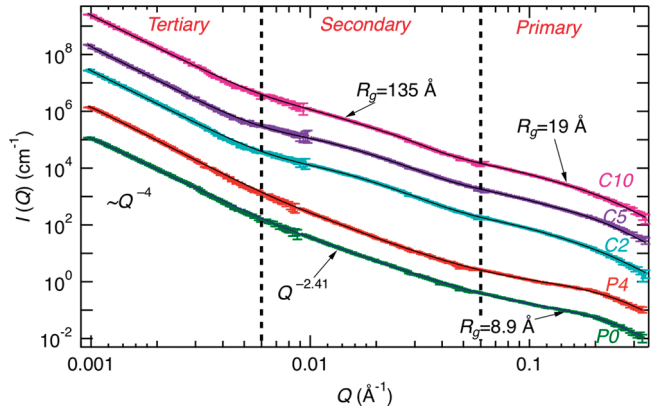

Figure 3. SANS studies of switchgrass dilute acid pretreated samples: (i) untreated, *P0*; (ii) presoaked for 4 h, *P4*; (iii) dilute acid treated at 160 °C for 2 min, *C2*; (iv) 5 min, *C5*; and (v) 10 min, *C10*. The solid lines are the unified fit to the experimental SANS data. The power-law exponent and the Guinier regime radius of gyration, R_g are indicated. The curves have been offset by increasing powers of 10 from the unscaled *P0* curve.

The SANS data of switchgrass as a function of pretreatment reaction time and temperature are shown in Figure 3. The curves show three distinct structural regimes defined here as primary, Q > 0.06 Å^{-1}, secondary, 0.006 Å^{-1} < Q < 0.06 Å^{-1}, and tertiary, 0.001 Å^{-1} < Q < 0.006 Å^{-1}. Each regime was fit by one level of the unified model[35−37] in eq 1, respectively. Hence, three levels of the unified fit were used to fit the three regimes. The solid black lines in Figure 3 are the fit results. All curves are similar in the tertiary regime, while clear differences exist in the primary and secondary regime between before (*P0*, *P4*) and after (*C2*, *C5*, *C10*) pretreatment protocol attains 160 °C. Differences between the untreated and presoaked or among different heat treated samples are subtle. Results of the component extracted switchgrass samples are summarized in Figure 4 with unified fits again shown as solid black lines. As observed for dilute acid pretreated samples, all scattering curves exhibit three distinct structural regimes with boundaries located at approximately Q = 0.006 Å^{-1} and Q = 0.06 Å^{-1}. The obtained structural parameters, that is, power law exponents P and characteristic dimensions R_g, from all unified fits are summarized in Table 2.

The most pronounced change in response to hot dilute acid pretreatment is the appearance of a new characteristic length scale described by an average radius of gyration (R_g) of 135 Å. This can be seen as a downward curvature in the secondary regime of samples *C2*, *C5*, and *C10* (Figure 3). This feature is absent from the untreated and presoaked switchgrass data, which instead show power law behavior in the same Q-range. Likewise, lignin removal by using lignin-component extraction treatment, as described in Materials and Methods after dilute sulfuric acid pretreatment, leads to disappearance of this characteristic

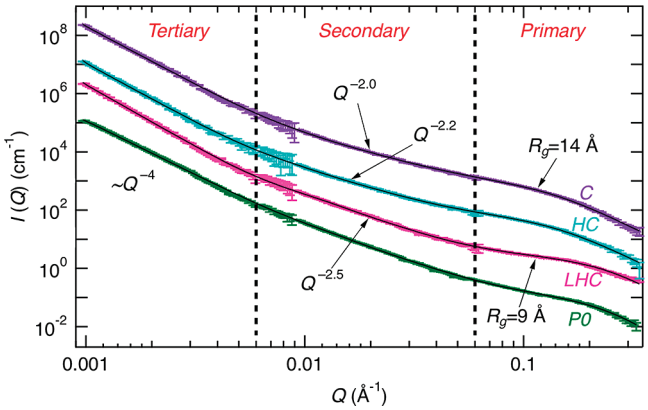

Figure 4. SANS studies of switchgrass component-extraction process samples: (i) untreated, *P0*; (ii) extractive-free, *LHC*; (iii) isolated holocellulose, *HC*; and (iv) isolated cellulose, *C*. The solid lines are the unified fit to the experimental SANS data. The power-law exponent and the Guinier regime radius of gyration, R_g are indicated. The curves have been offset by increasing powers of 10 from the unscaled *P0* curve.

Table 2. SANS Results of Dilute Acid Pretreatment and Component-Extracted Treatment Samples[a]

	primary		secondary		tertiary
samples	R_g (Å)	d (Å)	P	R_g (Å)	P
P0	8.9 ± 0.6	20.6 ± 1.4	2.41 ± 0.08		3.94 ± 0.04
Dilute Acid Pretreatment					
P4	8.7 ± 0.7	20.1 ± 1.6	2.48 ± 0.09		3.72 ± 0.03
C2	17.9 ± 1.7	41.3 ± 3.9		124 ± 7	3.86 ± 0.04
C5	19.0 ± 1.0	43.9 ± 2.3		133 ± 7	3.91 ± 0.04
C10	18.1 ± 2.2	41.8 ± 5.1		147 ± 17	3.78 ± 0.04
Component-Extracted Treatment					
LHC	8.43 ± 0.45	19.5 ± 1.0	2.56 ± 0.08		4.25 ± 0.05
HC	13.3 ± 0.6	30.7 ± 1.4	2.21 ± 0.08		4.07 ± 0.05
C	13.6 ± 1.0	31.4 ± 2.3	2.03 ± 0.09		3.99 ± 0.04

[a] R_g, radius of gyration; d, cross-sectional diameter; and P, power-law exponent.

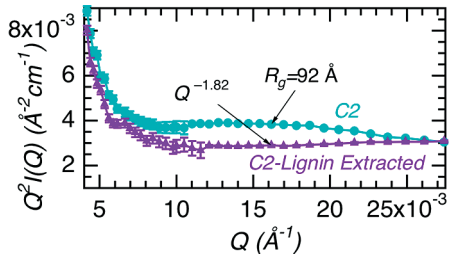

Figure 5. Kratky plot of SANS curves of dilute acid pretreated switchgrass at 160 °C for 2 min, *C2* (*i*) before (cyan dots) and (*ii*) after lignin extraction (purple dots). This plot displays only the secondary regime of the entire Q-range of Figure 3.

dimension. Figure 5, a Kratky plot[39,40] of $Q^2I(Q)$ versus Q shows the secondary SANS regime of two dilute acid pretreated (160 °C for 2 min) switchgrass samples: before (*C2*; cyan) and after (*C2-Lignin Extracted*; purple) lignin extraction. A Kratky plot enchances the appearance of characteristic particle sizes, which appear as broad peaks on a flat baseline. Figure 5 clearly shows that lignin extraction has eliminated the additional characteristic dimension as indicated by the removal of the peak on the approximately horizontal line. Such characteristic dimensions are also absent in the component-extracted samples (Figure 4), where lignin has been removed in the *HC* and *C* preparations. Detailed studies on this characteristic dimension growth during dilute acid pretreatment will be published elsewhere.[41]

SANS reveals power-law scattering at the secondary structural level for untreated, presoaked, and component extracted samples, where lignin aggregates are absent. Untreated and presoaked switchgrass shows power-law exponents of 2.4−2.5, suggesting the scattering signature of a highly branched biomass network of hemicellulose, cellulose, and lignin.[42] The degree of branching is reduced upon component extraction, approaching a power-law exponent of 2.0 for pure cellulose. For instance, a mass fractal with dimension $d_f \sim 2.5$ is observed for a randomly branched chain that follows a Gaussian path, while a non-branched Gaussian path has a fractal dimension $d_f \sim 2.0$.

In the tertiary regime, which is sensitive to length scales of about 1000 to 6000 Å, the data follows a power law with an exponent close to 4.0 (Table 2), indicating scattering from well-defined surfaces[43] (see Supporting Information, section *Scattering from Surfaces*). Dilute acid pretreatment up to 10 min at 160 °C does not change the SANS profile in the tertiary regime. To further examine biomass structure, the micrometer-scale morphology of switchgrass was probed by scanning electron microscopy. The SEM image clearly shows that well-defined cell wall surfaces remain present after pretreatment (Figure S1). Component extraction analysis adds further important results (Figure 4). The tertiary regime of sample *C* shows scattering from surfaces and is almost identical to untreated switchgrass. Cellulose is the only remaining biomass component after the final extraction step resulting in sample *C*, providing further evidence that the cellulose scaffold is able to hold up cell wall architecture when both lignin and hemicellulose are removed.

Distinct structural features at the smallest length scales are observed in the primary region of the SANS curves. These structural elements are described by a size parameter R_g, which approximately doubles during pretreatment from around 9 to 18 Å (Table 2). Comparison with component extracted sample *C* (Figure 4) shows that this characteristic length scale persists in the cellulose material after removal of all other components. An increase of about 50% in the primary size is observed in response to component extraction (Table 2).

Discussion

Our SANS results demonstrate that switchgrass undergoes significant morphological changes in response to dilute sulfuric acid pretreatment. These changes manifest at certain specific length scales and with a clear dependence on temperature and pretreatment time.

Lignin is well-known to self-aggregate into large particles,[23,24] and lignin aggregates larger than observed in our study have been revealed by microscopic methods performed by Donohoe and co-workers.[44] These workers described that translocation and redistribution of lignin can lead to formation of lignin droplets of various morphologies. We observe a new structural signature with an average R_g of 135 Å, which would correspond to an approximate particle diameter of 350 Å for spherical or similarly compact objects. This structural signature disappears when lignin is removed by solvent extraction following switchgrass pretreatment (Figure 5). We therefore attribute this structural feature to lignin and propose that lignin aggregates are present within the bulk pretreated material prior to the formation of larger lignin droplets resulting from lignin redistribution at a later stage. Lignin aggregates do not form at room temperature during 4 h of presoaking in dilute acid. They are evident in samples that have been treated for a short time at high temperature (160 °C, 2 min, *C2* sample). The size of the observed aggregates increases only slightly for longer pretreat-

ment times of 5 and 10 min (Table 2). Such a relatively sudden onset of aggregate formation suggests that a critical phase transition temperature may need to be exceeded for aggregates to form. For instance, the glass transition temperature of lignin is between 125 and 192 °C[45−47] and may play a role in the time and temperature dependence of aggregate formation. A detailed compositional analysis of the untreated switchgrass lignin[29] performed by Samuel et al., as well as other biomass types[48] has been reported. Further SANS studies on a more detailed set of samples taken at different time/temperature points of the pretreatment protocol will be required to test this hypothesis.

In agreement with our interpretation, chemical analysis shows removal of xylose (the major constituent sugar of hemicellulose) and an increase in the relative lignin and cellulose content of dilute acid pretreated switchgrass (see Table 1).[38] These compositional changes correlate well with the structural changes observed by SANS. In other words, hemicellulose is effectively removed by hydrolysis after a short duration of hot dilute acid pretreatment, while lignin and cellulose remains. Because both lignin redistribution and hemicellulose removal occur in the early stages of pretreatment, it appears likely that these two processes are kinetically interdependent and may be synergistic. Further, more detailed kinetic studies will be required to test this hypothesis.

Cellulose forms the main structural component in the cell wall and owing to its fibrous and partially crystalline nature provides a stable scaffold that allows large-scale organization into cell wall anatomy. The cellulose scaffold remains intact even when the composite material undergoes massive changes at molecular scales through lignin and hemicellulose removal by pretreatment or component extraction. The persistence of scattering from well-defined surfaces at length scales of 1000 to 6000 Å and during dilute acid pretreatment up to 10 min at 160 °C is suggested by the power-law dependence of the SANS data at small scattering vectors (tertiary regime). SEM confirms that well-defined cell wall surfaces, which could produce this signature remain present after pretreatement (Figure S1). At the same time, the chemical analysis of the samples[38] as well as SANS data at larger scattering vectors show clear changes in the composition and nanostructure of the cell wall material. Recent preliminary data[41] suggest that pretreatment times of 60 min or longer at 160 °C in dilute acid eventually degrade the cellulose network and alter cell wall surfaces at the micrometer scale.

At the secondary structural level in Figures 3 and 4, we observe power-law exponents of approximately 2.5 to 2, when the SANS signal is not dominated by scattering from lignin aggregates. A power-law exponent, P, of the range $1 < P < 3$ relates to the degree of branching or connectivity, observed in the lignocellulose mesh.[42] Hence, the observed change in the exponent implies that the component-extraction process alters the organization of the biopolymers from a highly branched arrangement (*P0* and *LHC*) to a low degree of branching (*HC* or *C*). Similarly, dilute acid pretreatment redistributes lignin and dissolves hemicellulose, and a more open nanostructure and improved access by cellulase enzymes may result. For example, a critical pore size of 51 Å was estimated from the known dimension of the main cellulase enzyme cellobiohydrolase I secreted by the fungus *Trichoderma reesei*.[49,50] The correlations between biomass pretreatment, pore size, and enzyme accessibility have been estimated by various experimental approaches.[50−57] Further, the correlations between biomass pretreatment and enzyme digestibility have been reported by Chung et al. as a 5-fold increase of cellulose conversion for dilute acid pretreated switchgrass using straight saccharification.[58]

A fibril diameter of about 21−42 Å, as can be extracted from our SANS data, is consistent with an elementary cellulose fibril (ECF) thickness of 20−30 Å reported in the literature.[13,59] The proposed model by Ding and Himmel[59] suggests that ECF consists of a bundle of 36 β-D-glucan chains with a crystalline core surrounded by disordered outer cellulose chain layers. The average diameter would range from 20 Å (crystalline core) to 44 Å (entire 36-chain ECF bundle). Considering the close agreement between SANS data and the expected value for an elementary cellulose fibril diameter, as reported in the literature, we propose that the cross section of crystalline cellulose microfibrils dominates the SANS data at short length scales (10−50 Å).

The observation of an approximate doubling of the primary R_g suggests in view of the model of Ding and Himmel[59] that dilute sulfuric acid pretreatment increases crystalline packing from the native crystalline core to the entire cross section of the ECF. Our observation of increased local cellulose ordering is supported by recent findings of an increase in degree of cellulose crystallinity and size of crystallites by NMR.[38,60]

The size of the primary structural units also increases in response to the component-extraction process. The R_g of the primary structural units from SANS (Table 2) reflects a 50% size increase between untreated and final extracted cellulose (*P0* to *C*). It is conceivable that crystalline packing of cellulose molecules may be less ordered in the native fibril due to competing hydrogen bond interactions with surrounding disordered cellulose and hemicelluloses, and pretreatment may remove such constraints and promote tighter packing of crystalline cellulose. Opposing mechanisms of cellulose disordering versus recrystallization under hydrothermal conditions have been reported previously[60] and conditions in hot dilute acid pretreatment could in fact promote cellulose "annealing".[61−63]

Conclusion

The present study provides insight into the consequences of dilute acid pretreatment of biomass from herbaceous crops by direct observation of the structural features over length scales from molecular distances to about 0.5 μm. SANS proved powerful in supplying the bulk of structural information presented here and we should emphasize that primary SANS results are obtained in terms of characteristic size parameters and morphological power-law signatures. The interpretation of these structural parameters and their attribution to individual components in the multicomponent biomass system is not unambiguous when based solely on the SANS profiles. It is therefore important to utilize complementary techniques and control experiments to confirm the specific conclusions, as was done in this study. The combined evidence of all our data as well as data published by other workers let us conclude that the scenario described by us is plausible; it uses a minimal set of hypotheses that are consistent with the data.

It is commonly accepted that lignin coating of cellulose fibrils and dense crystalline fibrous packing of cellulose are both factors that impede hydrolysis, and therefore, efficiency of pretreatment methods depends on a complex mixture of molecular processes. Our results suggest that temperatures in the vicinity of the glass transition of lignin lead to a rapid redistribution of lignin as well as dissolution of hemicellulose. Lignin is redistributed as distinct aggregates rather than forming a coating on cellulose fibrils as proposed previously.[10] It is suggested that hot dilute

sulfuric acid pretreatment of switchgrass biomass increases digestibility through lignin redistribution and through hemicellulose dissolution. A side-effect of hemicellulose removal and hydrothermal conditions is an annealing of cellulose that may increase crystallinity and may limit the efficiency of this pretreatment method.

Importantly, the structural network of cellulose does not show signs of breakdown, while lignin redistribution and hemicellulose removal are well under way early in the hot dilute acid pretreatment. Similarly, earlier studies of acid-pretreated and steam-exploded wood samples found little change in crystallinity of the cellulose and determined additionally that total surface area was not a controlling parameter.[50] Our results suggest that strategies for biomass pretreatment should clearly distinguish between targeting lignin/hemicellulose removal versus breakdown of crystalline cellulose fibrils.

Acknowledgment. Switchgrass samples were obtained through a collaborative agreement with the Bioenergy Science Center (BESC) located at the Oak Ridge National Laboratory, Oak Ridge, Tennessee. Paul A. Menchhofer and Kimberly Shawn Reeves are acknowledged for their assistance with generating SEM images. This research is funded by the Genomic Science Program, Office of Biological and Environmental Research, U.S. Department of Energy, under FWP ERKP752. Preliminary research was funded by an award (S07-019) from the Seed Money Fund of the Laboratory Directed Research and Development Fund, Oak Ridge National Laboratory. This research at Oak Ridge National Laboratory's Center for Structural Molecular Biology (CSMB) was supported by the Office of Biological and Environmental Research, using facilities supported by the U.S. Department of Energy, managed by UT-Battelle, LLC under Contract No. DE-AC05-00OR22725.

Supporting Information Available. SEM image and additional details on interpretation of scattering from surfaces. This material is available free of charge via the Internet at http://pubs.acs.org.

References and Notes

(1) Himmel, M. E.; Ding, S.-Y.; Johnson, D. K.; Adney, W. S.; Nimlos, M. R.; Brady, J. W.; Foust, T. D. Biomass Recalcitrance: Engineering Plants and Enzymes for Biofuels Production. *Science* **2007**, *315* (5813), 804–807.

(2) Lynd, L. R.; Cushman, J. H.; Nichols, R. J.; Wyman, C. E. Fuel Ethanol from Cellulosic Biomass. *Science* **1991**, *251* (4999), 1318–1323.

(3) Bouton, J. Improvement of Switchgrass as a Bioenergy Crop. *Genet. Improv. Bioenergy Crops* **2008**, 309–345.

(4) Bouton, J. H. Molecular Breeding of Switchgrass for Use As a Biofuel Crop. *Curr. Opin. Genet. Dev.* **2007**, *17* (6), 553–558.

(5) McMillan, J. D. In *Enzymatic Conversion of Biomass for Fuels Production*; Himmel, M. E., Baker, J. O., Overend, R. P., Eds.; American Chemical Society: Washington DC, 1994; pp 292−324.

(6) Adapted from "Genomics: GTL Transforming Cellulosic Biomass," U.S. Department of Energy Office of Science and Office of Energy Efficiency and Renewable Energy, June 2006, http://genomicscience.energy.gov/biofuels/, and U.S. DOE. 2006.

(7) Adapted from "Breaking the Biological Barriers to Cellulosic Ethanol: A Joint Research Agenda," DOE/SC/EE-0095, U.S. Department of Energy Office of Science and Office of Energy Efficiency and Renewable Energy, http://genomicscience.energy.gov/biofuels/.

(8) Coughlan, M. P. Cellulose Degradation by Fungi. In *Microbial Enzymes and Biotechnology*, 2nd ed.; Fogarty, W. M., Kelly, C. T., Eds.; Elsevier Applied Sciences: London and New York, 1990; Chapter 1.

(9) Zhang, Y.-H. P.; Himmel, M. E.; Mielenz, J. R. Outlook for Cellulase Improvement: Screening and Selection Strategies. *Biotechnol. Adv.* **2006**, *24* (5), 452–481.

(10) Zhang, Y.-H. P.; Lynd, L. R. toward an Aggregated Understanding of Enzymatic Hydrolysis of Cellulose: Noncomplexed Cellulase Systems. *Biotechnol. Bioeng.* **2004**, *88* (7), 797–824.

(11) Lee, I.; Evans, B. R.; Woodward, J. the Mechanism of Cellulase Action on Cotton Fibers: Evidence from Atomic Force Microscopy. *Ultramicroscopy* **2000**, *82* (1−4), 213–221.

(12) Fischer, E. W.; Herchenroder, P.; Manley, R. S. J.; Stamm, M. Small-Angle Neutron Scattering of Selectively Deuterated Cellulose. *Macromolecules* **1978**, *11* (1), 213–217.

(13) Jakob, H. F.; Fengel, D.; Tschegg, S. E.; Fratzl, P. The Elementary Cellulose Fibril in Picea abies: Comparison of Transmission Electron Microscopy, Small-Angle X-ray Scattering, and Wide-Angle X-ray Scattering Results. *Macromolecules* **1995**, *28* (26), 8782–8787.

(14) Jakob, H. F.; Tschegg, S. E.; Fratzl, P. Hydration Dependence of the Wood-Cell Wall Structure in Picea abies. A Small-Angle X-ray Scattering Study. *Macromolecules* **1996**, *29* (26), 8435–8440.

(15) Kawakatsu, T.; Tanaka, H.; Koizumi, S.; Hashimoto, T. Computer simulation of reaction-induced self-assembly of cellulose via enzymatic polymerization. *J. Phys.: Condens. Matter* **2006**, *18* (36), S2499–S2512.

(16) Kennedy, C.; Cameron, G.; Šturcová, A.; Apperley, D.; Altaner, C.; Wess, T.; Jarvis, M. Microfibril Diameter in Celery Collenchyma Cellulose: X-Ray Scattering and Nmr Evidence. *Cellulose* **2007**, *14* (3), 235–246.

(17) Nishiyama, Y.; Langan, P.; Chanzy, H. Crystal Structure and Hydrogen-Bonding System in Cellulose I_beta; from Synchrotron X-ray and Neutron Fiber Diffraction. *J. Am. Chem. Soc.* **2002**, *124* (31), 9074–9082.

(18) Nishiyama, Y.; Sugiyama, J.; Chanzy, H.; Langan, P. Crystal Structure and Hydrogen Bonding System in Cellulose I_alpha; from Synchrotron X-ray and Neutron Fiber Diffraction. *J. Am. Chem. Soc.* **2003**, *125* (47), 14300–14306.

(19) Tanaka, H.; Koizumi, S.; Hashimoto, T.; Kurosaki, K.; Kobayashi, S. Self-Assembly of Synthetic Cellulose During In Vitro Enzymatic Polymerization Process as Studied by a Combined Small-Angle Scattering Method. *Macromolecules* **2007**, *40* (17), 6304.

(20) Wada, M.; Kwon, G. J.; Nishiyama, Y. Structure and Thermal Behavior of a Cellulose I−Ethylenediamine Complex. *Biomacromolecules* **2008**, *9* (10), 2898.

(21) Wada, M.; Okano, T.; Sugiyama, J. Synchrotron-Radiated X-ray and Neutron Diffraction Study of Native Cellulose. *Cellulose* **1997**, *4* (3), 221–232.

(22) Norgren, M.; Edlund, H.; Wagberg, L. Aggregation of Lignin Derivatives under Alkaline Conditions. Kinetics and Aggregate Structure. *Langmuir* **2002**, *18* (7), 2859–2865.

(23) Vainio, U.; Maximova, N.; Hortling, B.; Laine, J.; Stenius, P.; Simola, L. K.; Gravitis, J.; Serimaa, R. Morphology of Dry Lignins and Size and Shape of Dissolved Kraft Lignin Particles by X-ray Scattering. *Langmuir* **2004**, *20* (22), 9736–9744.

(24) Woerner, D. L.; McCarthy, J. L. Lignin. 24. Ultrafiltration and light-scattering evidence for association of kraft lignins in aqueous solutions. *Macromolecules* **1988**, *21* (7), 2160–2166.

(25) Horii, F.; Yamamoto, H.; Kitamaru, R.; Tanahashi, M.; Higuchi, T. Transformation of native cellulose crystals induced by saturated steam at high temperatures. *Macromolecules* **2002**, *20* (11), 2946–2949.

(26) Kono, H.; Yunoki, S.; Shikano, T.; Fujiwara, M.; Erata, T.; Takai, M. CP/MAS ^{13}C NMR Study of Cellulose and Cellulose Derivatives. 1. Complete Assignment of the CP/MAS ^{13}C NMR Spectrum of the Native Cellulose. *J. Am. Chem. Soc.* **2002**, *124* (25), 7506–7511.

(27) Yamamoto, H.; Horii, F. CPMAS Carbon-13 NMR Analysis of the Crystal Transformation Induced for Valonia Cellulose by Annealing at High Temperatures. *Macromolecules* **2002**, *26* (6), 1313–1317.

(28) Hu, Z.; Sykes, R.; Davis, M. F.; Charles Brummer, E.; Ragauskas, A. J. Chemical Profiles of Switchgrass. *Bioresour. Technol.* **2010**, *101* (9), 3253–3257.

(29) Samuel, R.; Pu, Y.; Raman, B.; Ragauskas, A. Structural Characterization and Comparison of Switchgrass Ball-milled Lignin Before and After Dilute Acid Pretreatment. *Appl. Biochem. Biotechnol.* **2010**, *162* (1), 62–74.

(30) Esteghlalian, A.; Hashimoto, A. G.; Fenske, J. J.; Penner, M. H. Modeling and Optimization of the Dilute-Sulfuric-Acid Pretreatment of Corn Stover, Poplar and Switchgrass. *Bioresour. Technol.* **1997**, *59* (2−3), 129–136.

(31) Schell, D.; Farmer, J.; Newman, M.; McMillan, J. Dilute-Sulfuric Acid Pretreatment of Corn Stover in Pilot-Scale Reactor. *Appl. Biochem. Biotechnol.* **2003**, *105* (1), 69–85.

(32) Foston, M.; Hubbell, C.; Davis, M.; Ragauskas, A. Variations in Cellulosic Ultrastructure of Poplar. *BioEnergy Res.* **2009**, *2* (4), 193–197.

(33) Lynn, G. W.; Heller, W.; Urban, V.; Wignall, G. D.; Weiss, K.; Myles, D. A. A. Bio-SANS−a Dedicated Facility for Neutron Structural Biology at Oak Ridge National Laboratory. *Phys. B* **2006**, *385*−*386* (Part 2), 880–882.
(34) Ilavsky, J.; Jemian, P. R. Irena: Tool Suite for Modeling and Analysis of Small-Angle Scattering. *J. Appl. Crystallogr.* **2009**, *42* (2), 347–353.
(35) Beaucage, G. Approximations Leading to a Unified Exponential/Power-Law Approach to Small-Angle Scattering. *J. Appl. Crystallogr.* **1995**, *28* (6), 717–728.
(36) Beaucage, G. Small-Angle Scattering from Polymeric Mass Fractals of Arbitrary Mass-Fractal Dimension. *J. Appl. Crystallogr.* **1996**, *29* (2), 134–146.
(37) Belina, G.; Urban, V.; Straube, E.; Pyckhout-Hintzen, W.; Kluppel, M.; Heinrich, G. Microscopic Deformation of Filler Particles in Rubber under Uniaxial Deformation. *Macromol. Symp.* **2003**, *200* (1), 121–128.
(38) Foston, M. B.; Ragauskas, A. J. Changes in Lignocellulosic Supramolecular and Ultrastructure during Dilute Acid Pretreatment of Poplar and Switchgrass. *Biomass Bioenergy* **2010**, submitted for publication.
(39) Flory, P. J. *Statistical Mechanics of Chain Molecules*; Interscience Publishers: New York, 1969.
(40) Glatter, O.; Kratky, O. *Small Angle X-ray Scattering*; Academic Press: New York, 1982.
(41) Pingali, S. V.; Urban, V. S.; Heller, W. T.; McGaughey, J.; O'Neill, H. M.; Foston, M.; Myles, D. A. A.; Ragauskas, A.; Evans, B. R., Lignin Aggregate Growth during Dilute Acid Pretreatment of Lignocellulosic Biomass. **2010**, to be submitted for publication.
(42) Beaucage, G. Determination of Branch Fraction and Minimum Dimension of Mass-Fractal Aggregates. *Phys. Rev. E* **2004**, *70* (3), 031401.
(43) Paul, W. S.; David, A.; David, L.; Axel, H.; Mathias, S.; Armin, R. Small-Angle X-Ray Scattering from the Surfaces of Reversed-Phase Silicas: Power-Law Scattering Exponents of Magnitudes Greater than Four. *J. Chem. Phys.* **1991**, *94* (2), 1474–1479.
(44) Donohoe, B. S.; Decker, S. R.; Tucker, M. P.; Himmel, M. E.; Vinzant, T. B. Visualizing Lignin Coalescence and Migration through Maize Cell Walls Following Thermochemical Pretreatment. *Biotechnol. Bioeng.* **2008**, *101* (5), 913–925.
(45) Irvine, G. M. The Significance of the Glass Transition of Lignin in Thermomechanical Pulping. *Wood Sci. Technol.* **1985**, *19* (2), 139–149.
(46) Salmén, L. Viscoelastic Properties Ofin Situ Lignin under Water-Saturated Conditions. *J. Mater. Sci.* **1984**, *19* (9), 3090–3096.
(47) Shao, S.; Jin, Z.; Wen, G.; Iiyama, K. Thermocharacteristics of Steam-Exploded Bamboo (*Phyllostachys pubescens*) Lignin. *Wood Sci. Technol.* **2009**, *43* (7), 643–652.
(48) Sannigrahi, P.; Ragauskas, A. J.; Tuskan, G. A. Poplar as a Feedstock for Biofuels: A Review of Compositional Characteristics. *Biofuels, Bioprod. Biorefin.* **2010**, *4* (2), 209–226.
(49) Cantarel, B. L.; Coutinho, P. M.; Rancurel, C.; Bernard, T.; Lombard, V.; Henrissat, B. The Carbohydrate-Active Enzymes Database (CAZy): An Expert Resource for Glycogenomics. *Nucleic Acids Res.* **2009**, *37* (suppl_1), D233–238.
(50) Grethlein, H. E.; Converse, A. O. Common Aspects of Acid Prehydrolysis and Steam Explosion for Pretreating Wood. *Bioresour. Technol.* **1991**, *36* (1), 77–82.
(51) Brunecky, R.; Vinzant, T. B.; Porter, S. E.; Donohoe, B. S.; Johnson, D. K.; Himmel, M. E. Redistribution of Xylan in Maize Cell Walls during Dilute Acid Pretreatment. *Biotechnol. Bioeng.* **2009**, *102* (6), 1537–1543.
(52) Donohoe, B. S.; Selig, M. J.; Viamajala, S.; Vinzant, T. B.; Adney, W. S.; Himmel, M. E. Detecting Cellulase Penetration into Corn Stover Cell Walls by Immuno-Electron Microscopy. *Biotechnol. Bioeng.* **2009**, *103* (3), 480–489.
(53) Hong, J.; Ye, X.; Zhang, Y. H. P. Quantitative Determination of Cellulose Accessibility to Cellulase Based on Adsorption of a Nonhydrolytic Fusion Protein Containing CBM and GFP with Its Applications. *Langmuir* **2007**, *23* (25), 12535–12540.
(54) Igarashi, K.; Koivula, A.; Wada, M.; Kimura, S.; Penttil, M.; Samejima, M. High Speed Atomic Force Microscopy Visualizes Processive Movement of *Trichoderma reesei* Cellobiohydrolase I on Crystalline Cellulose. *J. Biol. Chem.* **2009**, *284* (52), 36186–36190.
(55) Matsushita, Y.; Yamauchi, K.; Takabe, K.; Awano, T.; Yoshinaga, A.; Kato, M.; Kobayashi, T.; Asada, T.; Furujyo, A.; Fukushima, K. Enzymatic Saccharification of Eucalyptus Bark Using Hydrothermal Pre-Treatment with Carbon Dioxide. *Bioresour. Technol.* **2010**, *101* (13), 4936–4939.
(56) Porter, S. E.; Donohoe, B. S.; Beery, K. E.; Xu, Q.; Ding, S.-Y.; Vinzant, T. B.; Abbas, C. A.; Himmel, M. E. Microscopic Analysis of Corn Fiber Using Starch- And Cellulose-Specific Molecular Probes. *Biotechnol. Bioeng.* **2007**, *98* (1), 123–131.
(57) Stone, J. E.; Scallan, A. M.; Donefer, E.; Ahlgren, E. In *Cellulases and Their Applications. In Advances in Chemistry Series 95*; Hajny, G. J., Reese, E. T., Eds.; American Chemical Society: Washington D.C., 1969; pp 219−241.
(58) Chung, Y.-C.; Bakalinsky, A.; Penner, M. Enzymatic Saccharification and Fermentation of Xylose-Optimized Dilute Acid-Treated Lignocellulosics. *Appl. Biochem. Biotechnol.* **2005**, *124* (1), 947–961.
(59) Ding, S.-Y.; Himmel, M. E. The Maize Primary Cell Wall Microfibril: A New Model Derived from Direct Visualization. *J. Agric. Food Chem.* **2006**, *54* (3), 597–606.
(60) Fahlén, J.; Salmén, L. Cross-Sectional Structure of the Secondary Wall of Wood Fibers as Affected by Processing. *J. Mater. Sci.* **2003**, *38* (1), 119–126.
(61) Debzi, E. M.; Chanzy, H.; Sugiyama, J.; Tekely, P.; Excoffier, G. The I$\alpha \rightarrow$Iβ Transformation of Highly Crystalline Cellulose by Annealing in Various Mediums. *Macromolecules* **1991**, *24* (26), 6816–6822.
(62) Lindgren, T.; Edlund, U.; Iversen, T. A Multivariate Characterization of Crystal Transformations of Cellulose. *Cellulose* **1995**, *2* (4), 273–288.
(63) Sannigrahi, P.; Ragauskas, A.; Miller, S. Effects of Two-Stage Dilute Acid Pretreatment on the Structure and Composition of Lignin and Cellulose in Loblolly Pine. *BioEnergy Res.* **2008**, *1* (3), 205–214.

BM100455H